www.acsnano.org

Portable Bulk-Water Disinfection by Live Capture of Bacteria with Divergently Branched Porous Graphite in Electric Fields

Xianfu Luo, Weigu Li, Zexi Liang, Yifei Liu, and Donglei Emma Fan*



Downloaded via UNIV OF TEXAS AT AUSTIN on August 29, 2023 at 22:29:47 (UTC). See https://pubs.acs.org/sharingguidelines for options on how to legitimately share published articles.

Cite This: ACS Nano 2023, 17, 10041-10054



ACCESS

Metrics & More

Article Recommendations

Supporting Information

ABSTRACT: Easy access to clean water is essential to functioning and development of modern society. However, it remains arduous to develop energy-efficient, facile, and portable water treatment systems for point-of-use (POU) applications, which is particularly imperative for the safety and resilience of society during extreme weather and critical situations. Here, we propose and validate a meritorious working scheme for water disinfection via directly capturing and removing pathogen cells from bulk water using strategically designed three-dimensional (3D) porous dendritic graphite foams (PDGFs) in a high-frequency AC field. The prototype, integrated in a 3D-printed portable water-purification



module, can reproducibly remove 99.997% *E. coli* bacteria in bulk water at a few voltages with among the lowest energy consumption at 435.5 J·L⁻¹. The PDGFs, costing \$1.47 per piece, can robustly operate at least 20 times for more than 8 h in total without functional degradation. Furthermore, we successfully unravel the involved disinfection mechanism with one-dimensional Brownian dynamics simulation. The system is practically applied that brings natural water in Waller Creek at UT Austin to the safe drinking level. This research, including the working mechanism based on dendritically porous graphite and the design scheme, could inspire a future device paradigm for POU water treatment.

KEYWORDS: water treatment, portable, porous graphite, dielectrophoresis, electroalignment

Tresh water in lakes, rivers, ponds, and streams has sustained the development of human societies for millions of years. However, most fresh water in nature does not meet today's drinkable standards set by the World Health Organization, particularly due to the presence of various disease-causing pathogens. The inadequate access to clean water has become an inflicting issue, not only in rural and developing areas, but also in modern cities. 1-5 The challenge is further compounded by the evident increase in frequencies and magnitude of extreme weather due to climate change.⁶ For instance, the winter storm in Texas in 2021 caused half of the state's population losing access to drinking water for days or weeks. The safety and sustainable development of society demand innovative technologies for water treatment in a robust, energy-efficient, cost-effective, and point-of-use (POU) manner.

A variety of water treatment techniques have been developed for large-scale water processing, such as reverse osmosis (RO), thermal distillation-based multistage flash and multieffect distillation, and electrodialysis that demand infrastructures and resources. Among these technologies, RO is often seen in home-based POU water treatment; however, it requires high water pressure and is susceptible to membrane fouling. 1,10,11 Recently, solar steaming (SS) with simple device

designs becomes promising for POU renewable water purification; 12-14 its performance depends on weather conditions and geographic locations, which is less accountable in challenging times, such as during extreme weather conditions. Also, intrinsically, solar steaming is a high energy-consuming technology, the working principle of which requires a large latent heat for the liquid-to-vapor phase transition. Chemical disinfection is simple and convenient; nonetheless, it uses strong oxidative agents, such as ozone, chlorine, and chlorine dioxide, which are hazardous to handle and could generate carcinogenic byproducts bringing dangers to people's health. 15,16

Electrochemical-mediated inactivation (EMI) has been explored for water treatment, which exhibits advantages owing to its facile scheme in lysing bacterial cells, removing heavy metals and organic contaminants, and self-cleaning.¹⁷

Received: December 8, 2022 Accepted: May 18, 2023 Published: May 24, 2023





When utilized for water disinfection, EMI operates mainly via mechanisms of electroporation and electrochemical oxidation; 18 the former requires the application of a high-intensity DC field (e.g., at 10⁷ V·m⁻¹) for damaging bacterial cells' membranes. ¹⁹⁻²¹ The latter requires electrochemically created species in an ionic solution for water disinfection. For instance, sulfate (Na₂SO₄) (50 mM sodium, 8.1 mS/cm) is used for improved electric conductivity supporting the electrochemical reactions. 22-24 Efforts have been made to modify electrodes with nanowires to amplify the localized electric field with the "lightning rod" effect so that it is possible to lyse bacteria with electroporation at a reduced DC voltage, e.g., <20 V.25-28 Silver, Cu₃P, and CuO nanowires have been synthesized on conducting surfaces for this purpose. 26-29 The application of a DC voltage, e.g., at only 1 V, can lyse cells, which, however, dissolves the nanowires and introduces metal ions to water. ^{26,30,31} In the demonstrations, the bacteria are mostly transported to the electrodes via forced flows with water pumping or stirring, which enables a high speed water process at the cost of POU complexity. The various electrochemically mediated methods are summarized in Table S1 in Supporting Information (SI). Indeed, both potential and challenges are present in this approach.

Notably, the recent advances in micro/nanomachines powered by external stimuli, including light, magnetic fields, and chemical fuels, have been applied in water treatment, including decontaminating bacteria. The designed structures and actuation mechanisms of micro/nanomachines demonstrate enhanced efficiency in interacting with substances in water compared to their static counterparts. Although such an approach is still largely at the proof-of-concept stage, e.g., treating water of a milliliter confined in a microwell, it inspires a different way of water purification.

In this work, we report a meritorious working principle, and the associated device scheme and materials for water disinfection. The method enables the physical removal of bacteria in contrast to cell lysis employed in many studies. The concept is based on manipulating bacterial cells via exploring the interaction between bacterial cells and high-frequency AC electric fields, created from strategically designed large-scale 3D porous dendritic graphite foam (PDGF). The bacteria can be mechanically aligned, transported, captured, and removed from bulk still water for water treatment. The working scheme demonstrates a successful removal of 99.997% Escherichia coli (E. coli) cells in 25 min with an energy consumption of only 435.5 J·L⁻¹, among the lowest of various water-disinfection technologies. The device is robust that shows no observable functional degradation after 20 repeated applications and can practically purify natural water from Waller Creek at UT Austin. Brownian dynamics simulation is carried out to shed light on the bacterial removal mechanism. The operation of the device does not require forced flows and is low-cost, durable, and scalable for portable water.

RESULTS AND DISCUSSION

Bacteria are widely present in fresh water, such as rivers, lakes, ponds, and streams. They include *Escherichia coli, Shigella, Salmonella enterica, Vibrio cholerae, Vibrio parahemolyticus,* and *Bacillus,* most of which can result in waterborne diseases. ^{35,36} Among various bacteria, due to the prevalence and the proportionality to other types of bacteria, *E. coli* is often used for evaluating water quality and water-treatment performance. ^{17,35–37} Therefore, we carry out systematic studies on

bacterial disinfection by using *E. coli* bacteria as a model system followed by the testing of shigella, another bacteria also widely found in natural water.

To capture bacteria from water, we explore the interactions between electric fields and the electrically polarized bacterial cells. When micro/nanoparticles are subjected to a high-frequency non-uniform AC electric field, they can be readily aligned and transported to either the highest or the lowest electric-field gradient. In water medium, the electric-field-particle interaction is governed by both the Maxwell–Wagner (MW) electric polarization of the micro/nanoobject and the electric double layer formed near the surface of the object in response to the MW polarization. The alignment torque (τ_e) in a uniform electric field, e.g., at a location far from two parallel electrodes, is given by eq 1^{38}

$$\tau_{e} = -\frac{1}{2}E_{0}^{2} \operatorname{Re}(\alpha_{\parallel} - \alpha_{\perp}) \sin \theta \cos \theta \hat{\mathbf{z}}$$
(1)

where E_0 is the amplitude of the electric field, α_\parallel and α_\perp are the total complex electric polarizability of the particle and electric double layer along the long and short dimensions, respectively, and θ is the angle between the long axis of the object and the electric field. In a nonuniform electric field, e.g., at a position close to the electrodes, a particle can be transported in the direction either toward or away from the highest electric field gradient, which depends on the relative electric polarization of the particle and the suspension medium. The associated force is the so-called dielectrophoresis (DEP). 39,40 A DEP force ($\langle F_{\rm DEP}(t) \rangle$) can be calculated as follows 41

$$\left\langle \mathbf{F}_{\mathrm{DEP}}(t) \right\rangle = \frac{1}{2} \mathrm{Re}(\underline{\alpha}) \nabla \mathbf{E}_{\mathrm{rms}}^{2}$$
 (2)

where $\underline{\alpha}$ is the complex total polarizability in the direction of the electric-field gradient for an object aligned by the field; it is determined by both the MW electric polarizability of the particle and the electric-double-layer polarizability. $E_{\rm rms}$ is the root-mean-square of the electric field intensity. When the AC frequency is above 100 kHz, the electric-double-layer effect can be considered negligible, ⁴¹ and the DEP force is determined by the MW electric polarization, depending on the electric conductivities and permittivities of both the micro/nanoobject and the water medium.

To this end, in microfluidic settings, an electric-field-based manipulation technique has been widely explored in transporting, aligning, rotating, separating, and sorting various micro/nanoentities, including biological cells, bacteria, and inorganic micro/nanowires, ribbons, spheres, and nanoporous structures. However, the manipulations that have been demonstrated are realized in a small region, usually a few hundreds of micrometers defined by the employed microelectrodes, and the volume is limited to milliliters to tens to hundreds of microliters, 40,42,43 which are not suitable for bulk water treatment. This is because when a physical dimension is changed, the dominating physics and challenges are often changed as well. It is intriguing to explore if the electric manipulation achieved on small scales can be utilized for macroscopic application. With the understanding of the challenge in this field and our in-depth knowledge of electric-field-material interactions, we proposed a device concept based on PDGF materials and an associated fabrication approach.

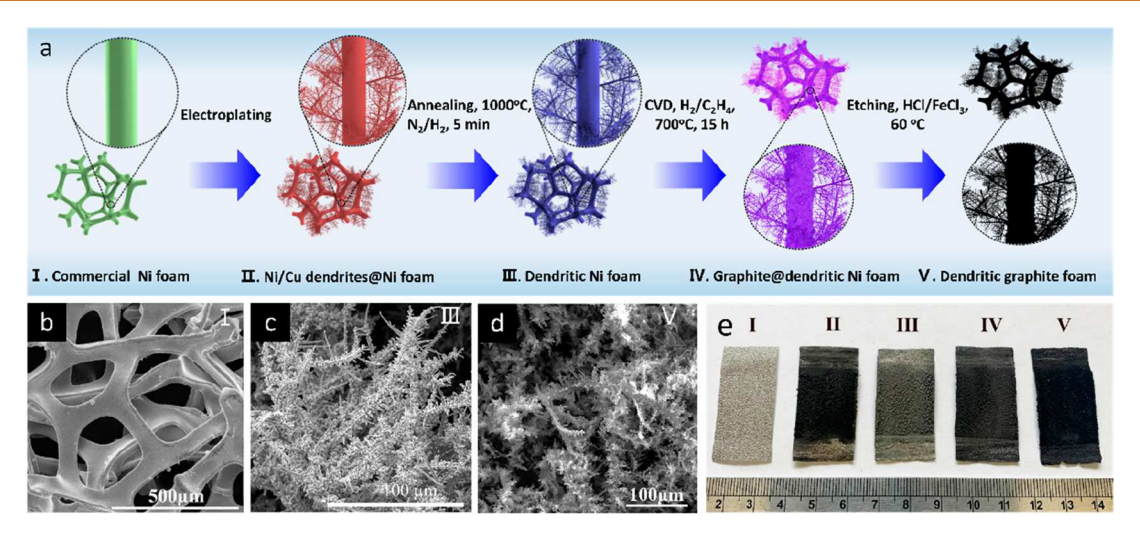


Figure 1. (a) Schematic of the fabrication process of dendritic graphite foams. Ni/Cu dendrites (II) are directly deposited on commercial Ni foams (I) via electroplating, followed by annealing at 1000 °C to strengthen the attachment strength between the dendrites and the Ni substrates (III). Thin graphite is grown on the dendritic Ni foam to replicate the branched morphology of the metallic foam (IV). Freestanding graphite foam (V) with replicated branched microstructures is finally obtained after chemical etching the Ni substrates. SEM images of (b) commercial Ni foams, (c) dendritic Ni foams, and (d) free-standing dendritic graphite foams. (e) Photographs of (I) commercial Ni foam, (II) Ni/Cu dendrites@Ni foam (before annealing), (III) Dendritic Ni foam (DNF, after annealing), (IV) graphite@dendritic Ni foam (GDNF, before etching), (V) free-standing dendritic graphite foam (DGF, after metal etching).

We begin the study by exploring the strong motion response of E. coli cells to a nonuniform AC electric field created from microelectrodes to show the feasibility in aligning, capturing, and releasing bacterial cells. As depicted in Figure S1 and Movie S1 (SI), when an AC voltage of 10 MHz is applied across two parallel microelectrodes, the E. coli cells quickly align in the electric-field direction, transport, and attach to the edges of the microelectrodes, the location of the highest electric-field gradient. In addition to the DEP forces that can effectively attract bacteria toward the microelectrodes, there are two other factors that govern the bacteria's transport behaviors: (1) the locomotion of *E. coli* without tumbling; (2) the passive diffusion of E. coli. The contribution of all these three factors will be evaluated and discussed based on the understanding obtained from Brownian dynamic simulation. We also note that upon the removal of the AC voltages, the *E*. coli cells can be readily released alive from the microelectrodes and resume their locomotion (SI Note 1.1).

The above experiments conducted on a scale of hundreds of micrometers provide understanding for our exploration in bulk-water disinfection with PDGF-materials-powered DEP manipulation. The research reported in this work for water disinfection is based on exploiting electroalignment and DEP forces generated by high-frequency AC electric field for the mechanical manipulation and physical removal of bacteria in bulk still water. The bacterial cells are aligned by the electric fields, swim toward an electrode, and get captured; the leverage of the bacterium's locomotion contributes to the device's low energy consumption. In addition, the system can be portable, where there is no need for pumped water flows (Table S1).

Materials Fabrication, Device Design, and Performance Characterization. The fabrication of the PDGF-materials utilized in bacterial capture starts with the electro-deposition of porous dendritic Ni foams (PDNFs), which are applied as the catalytic templates for the conformable growth of PDGFs via chemical vapor deposition (CVD). Freestanding PDGF is obtained after selectively etching the catalytic templates, as depicted in Figure 1a. The detailed fabrication

is included in the Methods. In brief, first, PDNFs are made by directly electrodepositing 3D diverging nickel–copper (Ni/Cu) microbranches on a commercial Ni foam [NF, Figure 1b,e (I), Figure S2]. The Ni/Cu microbranches grow densely on the entire 3D surface of the Ni foam in an electrolyte consisting of copper sulfate (CuSO₄, 0.0025 M), nickel chloride (NiCl₂, 0.1 M), and boric acid (H₃BO₃, 0.323 M) [Figure 1c,e (II)]. After thermal annealing to strengthen the obtained dendritic foam [Figure 1e (III)], thin graphite is synthesized conformably on the PDNF via a CVD reaction in a gas mixture of C_2H_4 (10 sccm) and H_2 (20 sccm) at 700 °C for 15 h [Figure 1e (IV)]. The PDNF serves as both the catalyst and the template. Finally, we obtain highly branched PDGF superstructures after etching the metal cores in a FeCl₃/HCl solution [Figure 1d,e (V)].

Different from previous research, 44 here, we carry out onestep fabrication of bimetal Ni/Cu microbranches on commercial Ni foams for the catalytic growth of 3D dendritically porous graphite. With systematic optimization, we obtain PDNFs with a series of distinct morphologies (Figure 2), ranging from low-density short-branched superstructures (Figure 2a,b) to high-density long-branched superstructures (Figure 2e,f). It is found that the branch formation exhibits a high correlation with the presence of Cu²⁺ ions (>0.001 M) in the nickel-chloride electrolyte $Ni^{2+} > 0.1$ M, Cl^{-} > 0.1 M) that leads to the ramified Cu-Ni superstructures deposited on the Ni foam. The morphology, length, diameter, and density of the Cu-Ni microbranches depend on a series of electroplating conditions, including applied electric potential, electrolyte composition and concentration, pH values, as well as electrodeposition time. For instance, after optimization, multitudes of long Ni-Cu microbranches with high aspect ratios (1–3 μ m in diameter, 100–200 μ m in length) can grow on the interconnected microstruts of the Ni foam (Figure 2e,f and Figure S3a-c). The as-obtained microbranches consist of uniformly distributing Ni (93.90 atom %) and Cu (6.10 atom %), as shown by the Energy-Dispersive X-ray spectroscopy (EDX) [Figure S4 and S5]. Both Ni and Cu are catalysts for

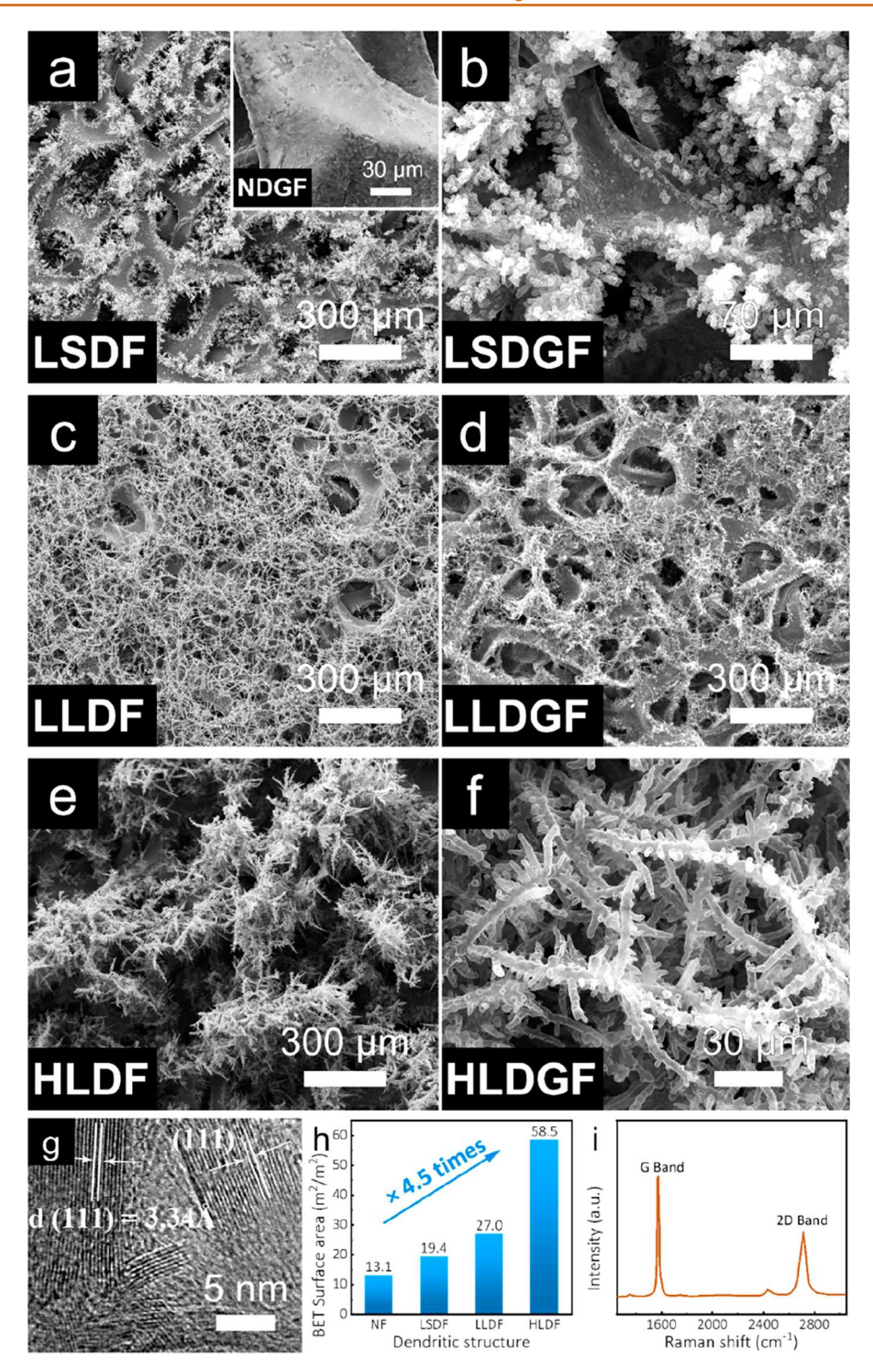
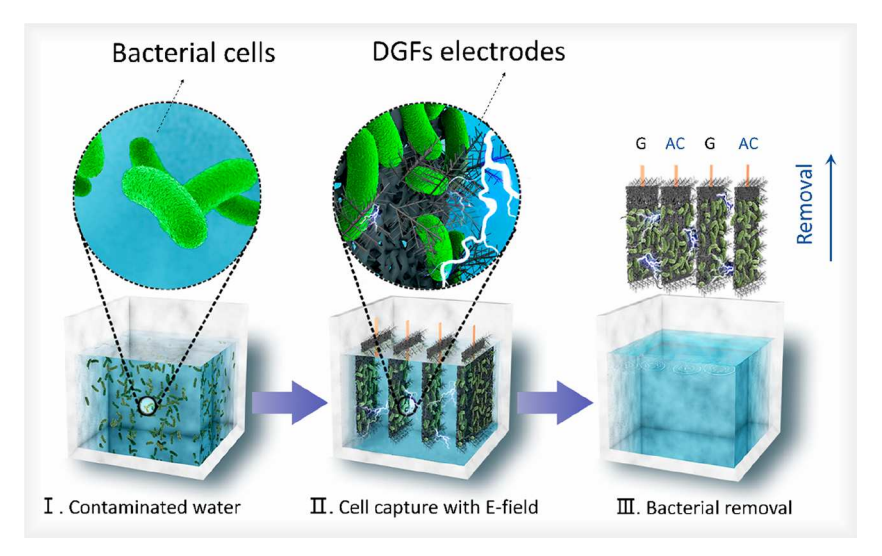


Figure 2. Characterization of the dendritic foams. SEM images of (a) low-density-short-branched dendritic foam (LSDF) [inset: nondendritic graphite foam (NDGF)], and the corresponding (b) low-density-short-branched dendritic graphite foam (LSDGF), (c) low-density-long-branched dendritic foam (LLDF) and the corresponding (d) low-density-long-branched dendritic graphite foam (LLDGF), (e) high-density-long-branched dendritic foam (HLDF, or dendritic Ni Foam, DNF) and the corresponding (f) high-density-long-branched dendritic graphite foam (HLDGF). Overall, the branched morphologies of DNFs are well preserved in the DGFs. (g) TEM image of DGFs. (h) Comparison of BET surface area test results of dendritic foams with different morphologies. NF: Ni foam; LSDF: low-density-short-branched dendritic foam; LLDF: low-density-long-branched dendritic foam. (i) Raman spectrum of DGFs.

graphene and thin graphite growth, and it is found the presence of Cu in Ni can consistently enhance the crystallinity and electric conductivity of thin graphite grown in the next step. 44–50 Furthermore, the diverging microbranches randomly

orient, extend, and fill the empty interconnected 3D microvoids of the 3D Ni foam. The fabrication of the microbranches not only increases the specific surface area of the template foam by 4.5 times, i.e., from 13.1 (Ni foam) to $58.5 \text{ m}^2/\text{m}^2$

Scheme 1. Schematic of Concept and Device Design of the AC-Electric-Field-Powered Dendritic Graphite Foams (DGFs) Electrodes for the Removal of Bacterial Cells from Contaminated Bulk Water



"The bacterial cells are captured and enriched on the DGFs electrodes with an applied AC electric field, and then removed from the water samples. AC: AC voltage and G: ground.

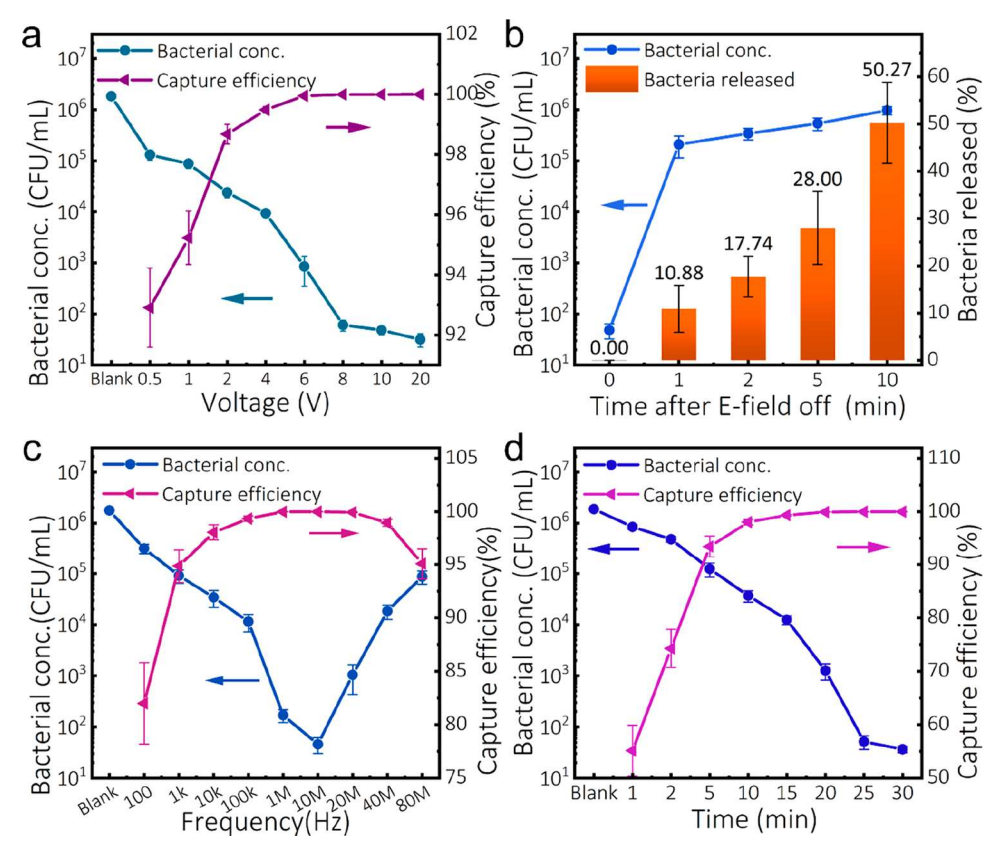


Figure 3. (a) Removal performance of *E. coli* cells increases as AC peak-to-peak voltage (10 MHz) increases. (b) Increases of the release bacteria with the off-time of electric field. Removal efficiency depends on (c) frequency (frequency below 100 Hz will be discussed separately) and (d) field application duration.

(PDNF) [Figure 2h], offering extensive 3D interfacial contact to bulk water in the bacterial disinfection applications, but also generates ultrastrong localized nonuniform electric fields due to the lightning-rod effect of the long microbranches;^{25–27} both advantages are essential for enhancing the interaction, attraction, and capture of bacterial cells from bulk water compared to that of planar electrodes.

Next, freestanding PDGFs are fabricated by conformable growth on the PDNF (Figure S3d-f) followed by selective etching of the PDNF template in a FeCl₃/HCl solution. The PDGFs offer large arrays of high-aspect-ratio tubular graphite microbranches covalently extended from the 3D porous graphite scaffold as shown in Figure 2f and Figure S3g-i. Compared to the smooth graphite foam obtained from simple

commercial Ni templates (Figure 2a inset, and Figure S6), the graphitic microtubes in PDGFs replicate the morphology of the diverging Ni/Cu microbranches. The graphite is highly crystalline and scalable that 2 cm × 4 cm samples can be routinely made in a research lab (HRTEM in Figure 2g, Figure S7, and Raman spectrum in Figure 2i). The fabrication only requires conventional electrodeposition and CVD techniques.

Finally, the obtained PDGFs are assembled in various configurations in a water-treatment module made by 3D printing (details in Methods). In a typical experiment, 4 identical PDGF electrodes are assembled in a cuboid container $(3 \times 1 \times 4, \text{ cm}^3)$ with an interdistance of 250 μ m. Next, a suspension of *E. coli* cells of ~10⁶ CFU/mL prepared in biological-grade water is dispersed in the container (Schematic 1), followed by the application of an electric signal of controlled voltage, frequency, and duration to the PDGF electrodes at room temperature (SI Note 1.2). The concentrations of bacteria before and after applying the electric field are determined by the standard spread-plate technique (details in Methods). The capture efficiency is calculated from the plate-counting numbers of bacterial colonies before and after the AC-voltage treatment.

It is found that at only 0.5 and 1 V (10 MHz and 25 min), this water treatment device can remove 92.910% and 95.230% bacterial cells, respectively. The efficiency further improves to 99.953% at 6 V and then reaches 99.998% at 20 V (Figure 3a). The results indicate that the strength of the electric field plays a salient role in removing the bacterial cells, agreeing with our understanding of the motion response of bacterial cells to a DEP force. We note that although the high-intensity AC field created by the highly branched porous foam could compromise the viability of bacteria, ~50% of bacteria recovered after we released the electric field for 10 min. Recovered cells monotonously increase with release time (Figure 3b). This study suggests that at the end of the 25 min AC-field application, where almost all the bacterial cells are caught by the dendritically porous electrodes, much of the population is alive. This result agrees with the aforediscussed observation of the microelectrode manipulation of bacteria, where after removing the high-frequency AC field, the bacterial cells captured on the electrodes restore their locomotion in solution. We further conduct a control experiment using a pair of Au-on-glass planar electrodes in the same experimental condition; immediately after the retrieval of the electrode set, we carry out the plate-counting test and observe almost no bacterial removal. This control experiment indicates that planar electrodes are effective in neither capturing and trapping nor lysing bacteria cells for bulk water treatment, highlighting the essential role of the dendritically porous superstructures as electrodes for powering efficient bacterial removal for water disinfection at low AC voltages. Indeed, previous works also show that a kilovolt-pulsed field is often required for cell lysis with electroporation in low-conductivity still water. 19,26,28,51 Overall, the experimental results obtained with the PDGF electrodes (Figure 2f-e) and planar microelectrodes (Figure S1) indicate that bacterial removal at the optimized 10 MHz is predominantly via DEP-force-assisted live cell capture owing to the highly branched porous electrodes, which has been realized on fresh still water using low AC electric voltages.

As we can achieve more than 95% disinfection at a voltage as low as 1 V, in the following, we choose a constant AC voltage at the same order of magnitude, i.e., 8 V, for systematic

characterization of the efficiency and energy consumption of the water disinfection system.

The bacterial removal depends on the AC frequency and is studied by varying the frequency from 100 Hz to 80 MHz. At each frequency, a constant AC voltage (8 V) is applied for 25 min. The efficiency rapidly increases between 100 Hz and 1 MHz and reaches a plateau at 1–20 MHz, and then slightly decreases in the range of 20 to 80 MHz (Figure 3c). The observed decrease can be attributed to the multiple shell structure of the bacteria, 52–55 where each shell has distinct dielectric properties that have been previously studied and modeled. The complex structure and variation in dielectric properties can lead to the DEP force/efficiency change at the high-frequency range.

The optimized AC frequency is in the range of 1-20 MHz, e.g., 99.997% at 10 MHz. Interestingly, when the AC frequency changes from 100 to 1 Hz, the device performance increases (Figure S8), though the disinfection is not effective as that at 10 MHz (same voltage and duration), and the working mechanism is distinct (SI Note 1.3).56 We notice that the application of DC or low-frequency AC signals often damages metal electrodes. For instance, Au microelectrodes can be easily damaged at approximately 3 V (SI Note 1.4, Figure S9). For the metallic porous dendritic Ni foams (PDNF) or graphite@dendritic Ni foam, even at a high frequency of 10 MHz where the electrochemical reaction can be substantially suppressed, the foams still undesirably release metallic ions that introduce ionic contaminants (SI Note 1.5, Figure S10). Indeed, it is imperative to employ graphite foams and AC voltages for contamination-free bacterial removal from water.

Next, we study how the efficiency of bacterial removal depends on the time of voltage application. The removal efficiency rapidly increases with time at 8 V, 10 MHz in the first 15 min (Figure 3d), before it gradually reaches 99.932% at 20 min and 99.998% at 30 min. The slow increase of the efficiency in the second 15 min can be attributed to the depletion of bacterial cells around the PDGF electrodes when most of them have been captured. The bacterial removal slowly approaches a plateau after 25 min; we consider 25 min as the effective removal time. The removal efficiency is almost the same for bacteria with concentrations from $\sim 3 \times 10^7$ to $\sim 2 \times 10^5$ CFU/mL (SI Note 1.6, Table S2).

It is highly interesting to understand how the disinfection efficiency depends on the morphologies of PDGF electrodes, i.e., the ramification degree and density of the microbranches. To address this question, we fabricate four types of 3D PDGFs, as well as a planar Au/Cr(50 nm/5 nm)-coated glass electrode as the control (Figure S11). After systematically tuning the electrodeposition parameters, including the concentrations of nickel chloride (NiCl₂) and copper sulfate (CuSO₄) in the electrolyte, we successfully obtain four types of PDGFs. They are low-density-short-branched DGFs (LSDGFs, Figure 2a,b), low-density-long-branched DGFs (LLDGFs, Figure 2c,d), high-density-long-branched DGFs (HLDGFs, Figure 2e,f), and nondendritic graphite foams (NDGFs, Figure 2a inset and Figure S6). The specific surface areas of the foams obtained via measurements of their templates are 19.4, 27.0, 58.5, and 13.1 m²/m², respectively (Figure 2h and Figure S12), where it can be found that the HLDFs offer the largest specific surface area, more than four folds of a commercial Ni foam. All 5 electrodes, including the four types of graphite foams and the Au/Cr glass, are tested at 8 V, 10 MHz for 25 min.

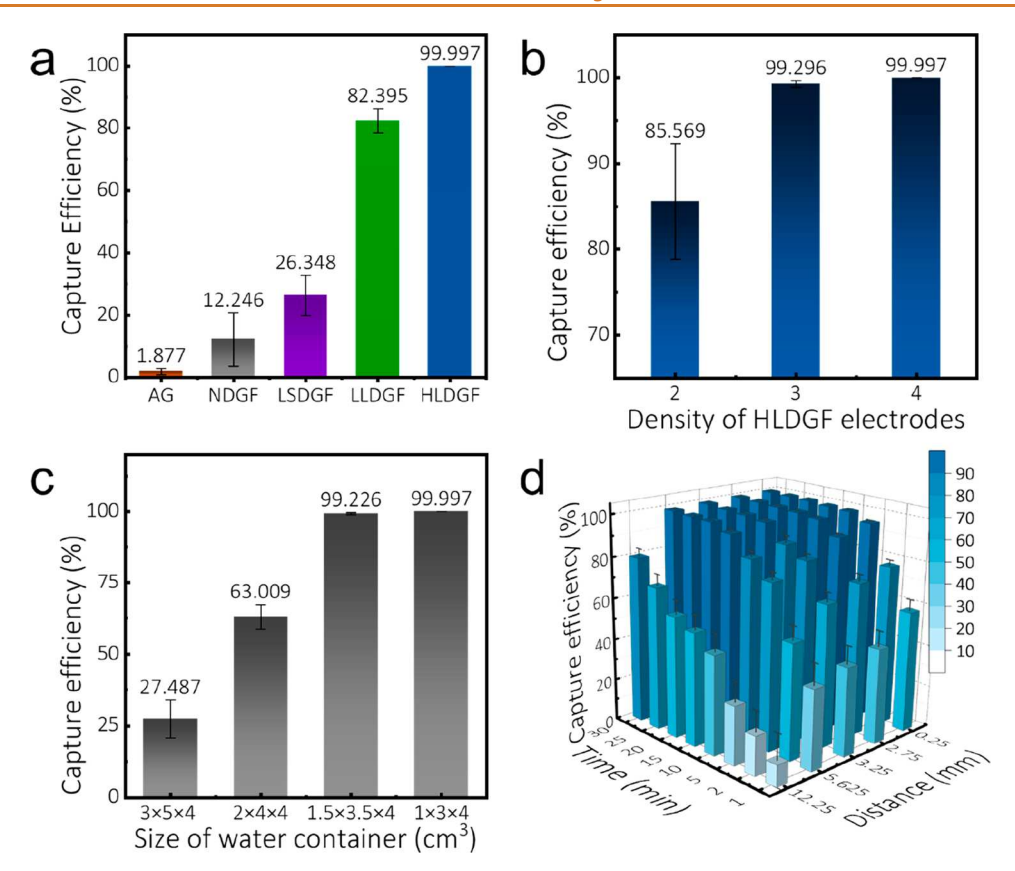


Figure 4. Removal efficiency of *E. coli* cells at 10 MHz, 8 V, depends on (a) morphology of DGFs electrodes (AG: planar Au-coated glass electrode for control experiment), (b) assembling density of DGFs electrodes, (c) volume of contaminated water, and (d) distance between DGFs electrode pairs.

As discussed earlier, the planar Au-on-glass electrode almost does not remove bacteria; the efficiency is only 1.877%. An improved but still rather low efficiency of 12.246% is obtained from the NDGFs electrode, the graphite foam made of smooth interconnected microstruts. In contrast, the ramified graphite electrodes with microbranched surfaces, LSDGFs, LLDGFs, and HLDGFs, demonstrate a greatly amplified effect in bacterial capture and removal. In particular, the HLDGFs with high-density long branches and the largest specific surface area offer the highest E. coli removal efficiency of 99.997%, followed by that of low-density-long-branched LLDGFs at 82.395%. The LSDGFs with low-density short branches show the lowest efficiency of 26.348% among the three ramified graphite foams (Figure 4a). These results unambiguously unveil the critical roles of the density and morphology of a dendritic foam for bacterial disinfection—the denser and longer the branches, the higher the bacterial removal efficiency.

Finally, we evaluate several important geometric factors of the water-treatment system, including the density of the HLGDF electrodes, volume of water, and electrode distance. It is found that the bacterial removal efficiency (Figure 4b) improves from 85.569% to 99.997% by simply increasing the number of HLGDF electrodes from 2 to 4 (8 V, 10 MHz). The efficiency also monotonically increases with the reduction of water volume, i.e., 27.487%, 63.009%, 99.226%, and 99.997% for water in containers of $3 \times 5 \times 4$, $2 \times 4 \times 4$, $1.5 \times 3.5 \times 4$, and $1 \times 3 \times 4$ cm³, respectively (Figure 4c). Furthermore, by reconfiguring the assembly of the HLDGFs electrodes to narrow their spacing (Figure S13), as shown in Figure 4d, consistent improvement of the bacterial removal

efficiency is obtained. In all tests, the removal of bacteria monotonically improves with the duration of electric-field application.

In addition to using *E. coli* as a model pathogen for water disinfection, we apply the same strategy for the removal of Shigella, another type of bacteria that is commonly found in natural bodies of water but does not exhibit similar locomotion as that of *E. coli* (Figure S14). Similar dependencies of removal efficiency on the distance, voltage, and time are observed, except that the frequency dependence is different from that of *E. coli* cells. At 1 kHz, the removal of Shigella is close to 100%.

Numerical Simulation: Shed Light on the Water Disinfection Mechanism. To gain insights into the working mechanism of the demonstrated bacterial removal, which is governed by the DEP force, bacterial locomotion, and passive diffusion, we carry out Brownian dynamic simulation. The simulation is built on a 1D Brownian dynamics model, and the aim is to provide understanding. The electric-field distribution is calculated by using COMSOL. Specifically, first, 100 000 bacteria are randomly seeded in the simulation domain between two electrodes. Each bacterium cell is then assigned a constant locomotion speed and direction. For E. coli cells, the locomotion speeds follow a Gaussian distribution with speed and deviation given by $\mu = 5.1 \ \mu \text{m/s}$ and $\sigma = 2.2 \ \mu \text{m/s}$, respectively, which are determined by experimental measurement in Figure S15a,b. The motion of each bacterial cell is governed by eq 3 in the following

$$\dot{X}(t) = \frac{D}{k_{\rm B}T} F_{\rm DEP}(X) + V_{\rm loco} + \sqrt{2D} R(t)$$
(3)

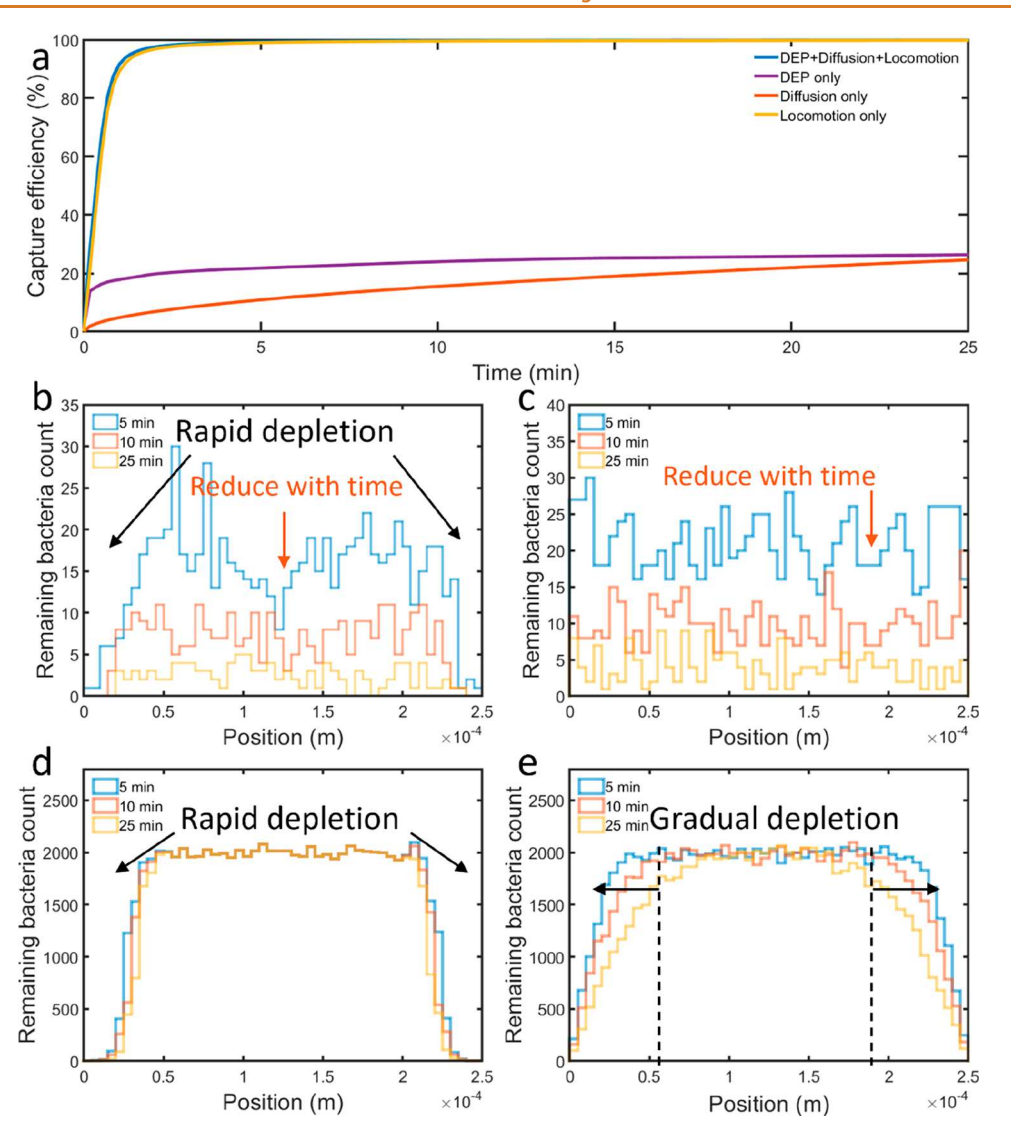


Figure 5. Brownian dynamics simulation result of bacteria purification in the $250 \, \mu m$ gap microelectrodes. (a) Capture efficiency versus time by diffusion, locomotion, DEP, and all three processes synergistically. (b-e) the untrapped bacteria distribution at different time stamps with (b) all three processes activated, (c) locomotion activated, (d) DEP activated, and (e) diffusion activated.

where X(t), D, $F_{\text{DEP}}(X)$, V_{loco} , and R(t) are the coordinate location, diffusivity of a bacterium, dielectrophoresis force, locomotion velocity of the E. coli, and a delta-correlated stationary Gaussian process that follows $\langle R(t) \rangle = 0$ and $\langle R(t) \rangle$ $R(t') = \delta(t - t')$. The time step, dt, is selected to be much larger than the relaxation time of a bacterium's Brownian motion, which guarantees that the simulation is overdamped. The detail is included in Supporting Information Note 2, which provides insights to the contributions of the three coexisting processes, i.e., bacterial locomotion, DEP attraction, and passive diffusion in water disinfection. It is found that the locomotion of bacteria makes the greatest contribution for the bacterial removal, which is assisted by the AC field alignment toward the electrodes (Figure 5a,b). The DEP attraction force is another salient process for bacteria removal, where it is most effective in the vicinity of the electrode of $\sim 50 \mu m$ (1D simulation) that rapidly depletes bacterial cells within the region and captures them on the microbranched porous electrodes (Figure 5c). For bacterial cells located beyond the DEP trapping region near the electrodes, they have to swim actively (Figure 5b) or diffuse passively into the trapping

regions to be captured by the electrodes (Figure 5d). The AC field alignment readily assists the swimming direction toward the electrodes, which enhances the bacterial capture efficiency. The simulation also suggests, for the nonmotile shigella, where the directional swimming is not viable as that in Figure 5b, that the disinfection mechanism at the optimized frequency of 1 kHz is different from that at 10 MHz. We note that strong electrokinetic flows occur at 1 kHz on electrodes; this effect could assist the transport of the bacteria cells in the center to the DEP-active region for trapping. Here, all the simulations are obtained from a 1D model, which facilitates understanding of the manipulation and contributing factors in the water treatment. To obtain quantitative insights, 3D simulation with sophisticated modeling of the ramified microelectrodes used in experiments is necessary.

The DEP-governed bacterial disinfection mechanism, as suggested in the simulation, is well supported by experimental observations (Figures 3 and 4). It is found that the efficiency of bacterial removal systematically increases with the applied voltage and time (Figure 3a,d), as well as the ramification and density of DGFs electrodes (Figure 4a,d).

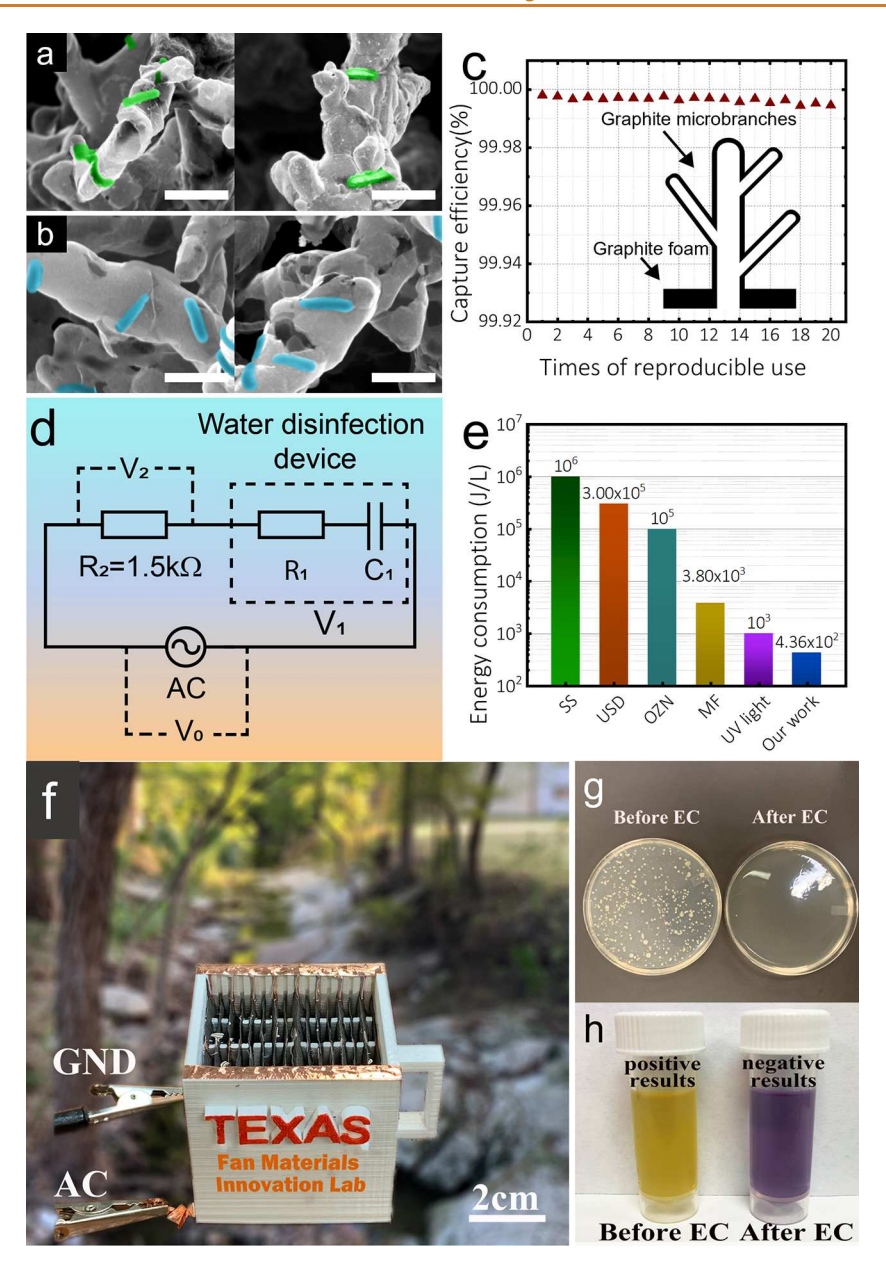


Figure 6. E. coli (a) and Shigella cells (b) in pseudocolors captured by a dendritic graphite foam. Scale bars in (a) and (b): 3 μ m. (c) Durability of the dendritic graphite foam in the efficient capture and removal of bacteria. Inset: Cross-section schematic of PDGF. (d) Diagram of test circuit for energy consumption. R_2 represents a known resistance of 1.5 k Ω , R_1 and C_1 together represent our water disinfection device. (e) Comparison of energy consumption of different bacterial disinfection approaches. (f) 125 mL portable disinfection cup applied for the disinfection of natural water collected from the Waller creek at UT-Austin, (g) cell culture results of water from the Waller creek before and after electric-field capture (EC), and (h) tests of bacteria in water from the Waller creek before and after electric-field capture. In yellow: bacterial positive; in purple: bacterial negative.

The simulation results also suggest that the DEP effect, much amplified by the highly branched HLGDFs electrodes, is distinct from DC-field-based electroporation that lyses bacteria via membrane disruption. Here the DEP force, generated via a low-voltage high-frequency AC electric field, disinfects water primarily by aligning, attracting, and capturing bacterial cells from contaminated water with the high-density-microbranched PDGFs. The PDGFs are essential in creating strong nonuniform AC electric fields that greatly intensify interactions with the bacterial cells in contrast to simple planar electrodes. This DEP-based bacterial manipulation, which has been studied using microscale electrodes in this and previous works (Figure S1), is now applied for bulk water treatment and proved to be

effective and advantageous in its low voltage and compatibility with freshwater in nature. ⁵⁸ As shown in the SEM images, after the water treatment, a large number of *E. coli* cells are found attaching to the microbranches of the PDGFs (Figure 6a and Figure S16a-c), as do Shigella cells (Figure 6b and Figure S16d-f). Here the PDGF electrodes are directly retrieved from water with applied AC voltages for the characterization.

Robust Device and Low Energy Consumption. Excellent robustness of the system is important for its practical use in water purification. We repeatedly employ the same system, i.e., the same PDGF electrodes and experimental conditions, for removing bacteria 20 times. The total working duration is more than 8.3 h, and we obtain over 99.990%

bacterial removal in all 20 tests (Figure 6c). This reliable performance can be attributed to the durable porous superstructures of the ramified PDGFs consisting of tubular microbranches covalently integrated with the 3D porous frameworks, as shown in Figure 6c inset. Scanning electron microscopy (SEM) imaging further confirms the well-maintained, highly ramified microstructures of the PDGFs after the 8.3 h application (Figure S17).

The next important performance is how well the watertreatment system operates in energy consumption. We evaluate this technical parameter at an optimized experimental condition. The testing circuit is constructed as shown in Figure 6d, in which the current and voltage can be measured at different locations in the circuit during water treatment, where V_0 , R_2 , R_1 , and C_1 are the applied voltage, external resistor of 1500 Ω , and measurable resistance and capacitance, respectively. An energy consumption of 435.5 J/L is determined (SI Note 1.7). This value is several orders-ofmagnitude lower compared to those of various cutting-edge water disinfection technologies that have received immense research interest, including solar steaming (SS, 10⁶ J·L⁻¹),⁵⁹⁻⁶¹ ultrasound disinfection (USD, $\sim 3 \times 10^{5}$ J·L⁻¹), ^{62,63} ozonation (OZN $1.3 \times 10^3 - 1.0 \times 10^5 \text{ J} \cdot \text{L}^{-1}$), 64–66 membrane filtration (MF, $6.8 \times 10^2 - 3.8 \times 10^3 \text{ J} \cdot \text{L}^{-1}$), 67–69 and ultraviolet light disinfection (UV light, ~ 1 to 3×10^3 J·L⁻¹) [Figure 6e]. $^{70-73}$ The advantageous low energy consumption can be attributed to the working principle exploited in this system, where the electric energy is largely used for physically aligning and translocating bacterial cells in water to electrodes. In comparison, for instance, the various solar-steaming techniques that have received remarkable attention require intrinsically high energy consumptions that involve liquid-to-vapor phase transition of water with an enthalpy of 2.46×10^6 J/L (44.2 kJ· $\mathrm{mol^{-1}}$, 101 325 Pa, 25 °C). The measured energy consumption suggests that even by utilizing a standard solar panel with an energy-conversion efficiency of 10%, the reported waterdisinfection module consumes much less energy than most of the aforediscussed technologies, which is desirable in addition to its advantageous portable bulk-water treatment.

Disinfection of Natural Water from the Waller Creek at UT Austin. Finally, confirming the validity and applicability of the working principle and device scheme with the systematic characterization, simulation, and understanding, we develop a water-disinfection prototype powered by low-voltage AC field for natural water treatment. In the past 4 years, the E. coli pollution of Waller Creek at UT Austin indicates a high level of bacterial pollution, as shown in Figure S18. For disinfecting water in Waller Creek, we make a portable water-disinfection cup $(5 \times 5 \times 5 \text{ cm}^3)$ by 3D printing and integrate it with multiple DGF electrodes as a device prototype (Figure 6f, Figure S19). The various bacterial colonies on the nutrient agar culture medium indicate the presence of different types of bacteria in the water sample. After the application of an ACvoltage at 10 MHz, 8 V for 25 min, almost no bacterium colony can be cultured on the counting plate (Figure 6g). This result is further confirmed by testing with commercial bacterial kits (Figure 6h). Indeed, the designed water treatment cup can practically disinfect bacterium-contaminated fresh water in nature. In addition, no soluble mineral in river water deposits on the PDGF electrodes (Figure S20, Supporting Information Note 1.8) after the AC voltage treatment.

The cup is compact and can be easily produced at a low cost with the synthesis of a PDGF electrode at only \$1.47 in a

laboratory condition (SI Note 1.9). We also designed a flow cell with a glass-pot appearance that allows for both water treatment and practical use (Figure S21). This design enables easy filling and pouring of water after treatment. In addition, for practical applications, we suggest a general method for choosing the optimized AC frequency considering water source, different bacterium types, and energy consumption (SI Note 1.10).

CONCLUSIONS

In summary, we propose and successfully validate a meritorious scheme for bacterial disinfection and the associated materials and device prototype for future portable applications. The research is achieved by exploiting the interaction of bacterial cells with nonuniform AC electric fields created via ramified graphite foams. As low as a few volts can effectively disinfect 99.997% E. coli bacteria in bulk water. Brownian dynamics simulations further unveil the critical role of the highly nonuniform AC electric field supported by the strategically designed ramified graphite foams, which directs bacterial locomotion toward the electrodes and creates highintensity near-field zones for cell capture. This working principle is different from the reported EMI technologies, where our device operates at low AC voltages in still water without any requirement for ionic additions or forced water flows. It has a simple device scheme, desirable for POU application. Among various emerging technologies, including chlorine disinfection, UV radiation, ozonation, and solar steaming, the water-disinfection system in this report requires an energy consumption of only 435.5 J·L⁻¹. Here, the biological energy of swimming bacterial cells also, in principle, contributes to the low energy cost. The system's operation does not have restrictions in geographical location or weather condition. Combined with the simple, portable, low cost, and robust performance, the system could find uses in extreme weather and events.

In this work, the device scheme focuses on the removal of bacteria in water. Based on the same setup, different working mechanisms could be explored to remove various types of micro/nanoobject, heavy metals, and organic contaminates. For instance, as aforediscussed, metals cannot directly deposit on electrodes by the high-frequency AC field. Nevertheless, a DC field can be explored based on the established electrodeposition methods as reported previously. In terms of micro/nanoobjects with a similar size of the bacterial cells, we expect that the same DEP mechanism can be applied for their purification. In terms of organic contaminants, previous work has demonstrated their oxidization and decontamination in a DC field, the so-called electrooxidation.

Finally, we design and fabricate a prototype water disinfection cup that successfully brings natural water in the Waller Creek at UT Austin to the safe level. Overall, this research could inspire the development of a class of water disinfection systems with distinct advantages for POU applications.

METHODS

Fabrication of Porous Dendritic Ni Foams (DNFs). The DNFs (HLDFs) were synthesized and electrodeposited successfully on commercial nickel foam substrates. Before electrodeposition, a piece of rolled commercial nickel foam (CNF, 2×4 cm², $200~\mu m$ in thickness, MTI Corporation, CA, USA) was successively washed with acetone, sulfuric acid (H_2SO_4 , 3~M), and DI water to completely

remove the surface oxide layer. Then, the diverging Ni-Cu microbranches were electrodeposited at -1.4 V (vs Ag/AgCl) for 150 C from an electrolyte constituted of copper sulfate (CuSO₄, 0.0025 M), nickel chloride (NiCl₂, 0.1 M), and boric acid (H₃BO₃, 0.323 M) with nickel foil (Alfa Aesar, MA, USA) working as the counter electrode on an electrochemical workstation (VersaSTAT 3, AMETEK Scientific Instruments). The electrodeposition was repeated 4 cycles with the CNF substrate rotated upside-down each time to guarantee uniform coverage of the ramified branches on the CNF substrate. Electrolyte compositions of the different porous structures: LSDF: CuSO₄, 0.001 M, NiCl₂, 0.1 M, and H₃BO₃, 0.323 M; LLDF: CuSO₄, 0.0025 M, NiCl₂, 0.025 M, and H₃BO₃, 0.323 M. The resultant DNFs were rinsed with DI water and ethanol, and then dried overnight in a vacuum dryer. After completely drying, the DGFs samples were rapidly annealed for 5 min at 1000 °C in a tube furnace (Lindberg/Blue M Mini-Mite Tube Furnaces, Thermo Scientific) with a gas flow of hydrogen (H2, 5 sccm) and nitrogen (N2, 50 sccm) of about 440 mTorr to improve the mechanical adhesion strength between the ramified microbranches and the nickel foam substrates.

Growth of Porous Dendritic Graphite Foams (DGFs) with **DNFs as Templates.** The graphite@dendritic Ni foams (GDNFs) are grown via CVD in a gas mixture of C2H4 and H2 at flow rates of 10 sccm, 20 sccm, respectively, at 700 °C. The reaction starts with the preparation of the surface of the dendritic Ni foam (DNFs) via reduction in H₂ gas flow (20 sccm) at 700 °C for 40 min to remove the surface oxides. Next, ethylene (C₂H₄, 10 sccm) is utilized as the carbon source to grow ultrathin graphite film on the DNFs catalysts with a total pressure of 400 mTorr for 15 h. Then, the temperature is rapidly reduced to room temperature in the original growth gas mixture. GDNFs are obtained with a layer of thin graphite conformably coated on the DNFs. Free-standing DGFs, which well replicate the porously branched superstructures of the DNFs, are obtained via selective chemical etching of the metal foam core in a $FeCl_3/HCl$ mixture ($FeCl_3/HCl = 1 M/2M$). The resultant ultrathin graphite foam is carefully rinsed with deionized water and isopropanol, and finally dried at 60 °C for 4 h. Finally, the DGFs are treated with hydrophilic in nitric acid (HNO₃, 4 M) at 50 °C for 2 h, followed by rinsing with DI water and isopropanol.

Water-Disinfection Device: Design and Fabrication. The construction of the water-disinfection device starts with the assembly of 4 pieces of GDNFs with an interdistance of 250 μ m into slots of a cuboid container (3 × 1 × 4 cm³) made by a 3D printer (MakerBot Replicator fifth Generation), followed by the selective chemical etching of the Ni core in FeCl₃/HCl mixture (FeCl₃/HCl = 1 M/2 M) and deionized-water washing to obtain the DNFs. Various arrangements of the DGFs are configured in both the horizontal and vertical directions of the water container (Figure S13). An electrically conductive copper tape is attached to one end of each piece of DNF, serving as the current collector. To protect the copper tape during the chemical etching of the Ni core of the foam, a layer of polydimethylsiloxane (PDMS) made of a mixture of base and curing agent (mass ratio of 10:1) is evenly coated on its surface followed by degassing in vacuum for 1 h and curing at 65 °C for 2 h.

Materials Characterization. The voltage supply for water treatment is provided by a function generator (Agilent 33250A). In order to calculate the energy consumption of our water treatment device, the measurement of the voltage and current of our device is carried out with an oscilloscope (Tektronix TDS 2024B). The working circuit for the test is shown in Figure 6d. The morphologies and microstructures of DNFs and DGFs are successively characterized by scanning electron microscopy (SEM, Hitachi S5500) equipped with energy dispersive spectroscopy (Bruker), Raman spectroscopy (customized setup with ultrasensitive CCD camera from Princeton instrument Inc.) and high-resolution transmission electron microscope (TEM, JEOL 2010F).

Bacterial Characterization. Commercial Escherichia coli (E. coli) solution (Carolina biological supply) is diluted 1000 times to $\sim 10^6$ CFU/mL (colony forming unit) with biological-grade water (Cat. No. W4502–1L, Sigma-Aldrich). The diluted bacterial suspension is transferred to the water treatment device. During the water treatment,

a constant electric voltage is applied to the DGFs electrodes via a functional generator. The characteristics of the applied electric field, i.e., AC voltage and frequency, DC voltage, and application duration are optimized to achieve excellent disinfection efficiency. Next, the treated water samples are collected with the electric voltage on. The DGFs are cleaned by large amounts of 75 vol % alcohol and DI water and stored for the next use. The bacterial concentrations of the processed suspensions and control samples are measured by using the standard spread plating techniques: 20 g solid agar (BP1423-500, Fisher) is dissolved in 500 mL DI water in a conical flask, which is then placed into an oven at 120 °C for 2 h to obtain the agar solution. Next, 20 mL agar solution is transferred to a Petri dish with a diameter of 80 mm. The Petri dish is then placed into a CO2 incubator (MCO-17AC, SANYO) at 37 °C for 12 h to obtain the solidified agar medium. For the bacteria culture, each water sample is serially and accurately diluted. Then, a 400 μ L diluted water sample is transferred to the Petri dish containing presolidified agar, and an Lshaped glass rod is utilized to smear the solution to spread on the agar surface. At last, the plates are transferred to a CO₂ incubator with 5.0 vol % CO2 and cultured at 37 °C for about 20 h. The bacterial concentration in the water sample can be calculated through the number of the bacterial colonies, dilution ratio, and water volume. Note that the use CO₂ is for maintaining the pH value of the solution. It is not necessary for the culture of *E. coli* cells but can be needed for other types of bacterial cells. As we tested the application of the device for the removal of bacteria from Waller creek, we controlled the pH value with the standard 5% CO₂ technique.

The motions of bacterial cells on the microelectrodes are observed with an inverted optical microscope (Olympus IX 71). To determine *E. coli* cells captured by the DGFs electrodes with SEM imaging, after water treatment, the DGF are collected and immersed overnight in 2.5% glutaraldehyde solution (Sigma-Aldrich) at 4 °C for cell fixing. Then the samples are rinsed 3 times with 0.1 M, pH 6.6 phosphate buffer solution (Sigma-Aldrich), successively dehydrated by a gradient of ethanol/water solutions (30%, 50%, 70%, 80%, 90%, 95%, and 100% wt, 15 min for each time), and dried in air. Bacterial tests for the treatment of natural water are performed with water testing kits (Test Assured).

ASSOCIATED CONTENT

Supporting Information

The Supporting Information is available free of charge at https://pubs.acs.org/doi/10.1021/acsnano.2c12229.

Movie S1 showing locomotion of bacterial cells under an AC electric field created from Au microelectrodes (MP4)

Discussion of locomotion of bacterial cells in fluids, temperature effects on bacterial removal, disinfection efficiency in low AC frequencies, DC voltage effect on metal electrode, reliable performance of dendritic graphite for bacterial disinfection, disinfection efficiency at different bacterial concentrations, calculation of energy consumption, mineral deposition on electrodes in a high-frequency AC field, calculation of cost, methods for determining the optimized AC frequency, and Brownian dynamics simulation details. Supplementary figures are included. (PDF)

AUTHOR INFORMATION

Corresponding Author

Donglei Emma Fan − Materials Science and Engineering Program and Department of Mechanical Engineering, The University of Texas at Austin, Austin, Texas 78712, United States; orcid.org/0000-0002-4724-2483; Email: dfan@austin.utexas.edu

Authors

- Xianfu Luo Materials Science and Engineering Program, The University of Texas at Austin, Austin, Texas 78712, United States
- Weigu Li Department of Mechanical Engineering, The University of Texas at Austin, Austin, Texas 78712, United States
- Zexi Liang Materials Science and Engineering Program, The University of Texas at Austin, Austin, Texas 78712, United States; orcid.org/0000-0001-9309-4496
- Yifei Liu Materials Science and Engineering Program, The University of Texas at Austin, Austin, Texas 78712, United States; ^⑤ orcid.org/0000-0003-0247-1247

Complete contact information is available at: https://pubs.acs.org/10.1021/acsnano.2c12229

Author Contributions

*W.L. and Z.L. contributed equally.

Notes

The work has previously been made available as a preprint: Luo, X.; Li, W.; Liang, Z.; Liu, Y.; Fan, D. Portable Bulk-Water Disinfection by Live Capture of Bacteria with Divergently Branched Porous Graphite in Electric Fields. November 14, 2022, *ChemRxiv*. 10.26434/chemrxiv-2022-kq39d.

The authors declare no competing financial interest.

ACKNOWLEDGMENTS

The authors are grateful for the support from the National Science Foundation (grant #1563382). The UT-Austin Portugal Pilot Program in 2021, and the Welch Foundation (F-1734).

REFERENCES

- (1) Shannon, M. A.; Bohn, P. W.; Elimelech, M.; Georgiadis, J. G.; Mariñas, B. J.; Mayes, A. M. Science and Technology for Water Purification in the Coming Decades. *Nature* **2008**, 452 (7185), 301–310.
- (2) Mullin, M. The Effects of Drinking Water Service Fragmentation on Drought-Related Water Security. *Science* **2020**, *368* (6488), 274–277.
- (3) Werber, J. R.; Osuji, C. O.; Elimelech, M. Materials for Next-Generation Desalination and Water Purification Membranes. *Nat. Rev. Mater.* **2016**, *1* (5), 1–15.
- (4) Amrose, S.; Burt, Z.; Ray, I. Safe Drinking Water for Low-Income Regions. Annu. Rev. Environ. Resour. 2015, 40 (1), 203-231.
- (5) Sadoff, C. W.; Borgomeo, E.; Uhlenbrook, S. Rethinking Water for SDG 6. Nat. Sustain. 2020, 3 (5), 346-347.
- (6) Guidelines for Drinking-Water Quality: 4th ed. Incorporating the First and Second Addenda; WHO Guidelines Approved by the Guidelines Review Committee; World Health Organization: Geneva, 2022.
- (7) Schwarzenbach, R. P.; Escher, B. I.; Fenner, K.; Hofstetter, T. B.; Johnson, C. A.; von Gunten, U.; Wehrli, B. The Challenge of Micropollutants in Aquatic Systems. *Science* **2006**, *313* (5790), 1072–1077
- (8) Zhang, M.; Xie, X.; Tang, M.; Criddle, C. S.; Cui, Y.; Wang, S. X. Magnetically Ultraresponsive Nanoscavengers for Next-Generation Water Purification Systems. *Nat. Commun.* **2013**, *4* (1), 1866.
- (9) Cohen-Tanugi, D.; McGovern, R. K.; Dave, S. H.; Lienhard, J. H.; Grossman, J. C. Quantifying the Potential of Ultra-Permeable Membranes for Water Desalination. *Energy Environ. Sci.* **2014**, 7 (3), 1134–1141.
- (10) Van der Bruggen, B.; Vandecasteele, C. Distillation vs. Membrane Filtration: Overview of Process Evolutions in Seawater Desalination. *Desalination* **2002**, *143* (3), 207–218.

- (11) Wenten, I.G.; Khoiruddin. Reverse Osmosis Applications: Prospect and Challenges. *Desalination* **2016**, 391, 112–125.
- (12) Li, W.; Li, Z.; Bertelsmann, K.; Fan, D. E. Portable Low-Pressure Solar Steaming-Collection Unisystem with Polypyrrole Origamis. *Adv. Mater.* **2019**, *31* (29), 1900720.
- (13) Tao, P.; Ni, G.; Song, C.; Shang, W.; Wu, J.; Zhu, J.; Chen, G.; Deng, T. Solar-Driven Interfacial Evaporation. *Nat. Energy* **2018**, 3 (12), 1031–1041.
- (14) Min, X.; Zhu, B.; Li, B.; Li, J.; Zhu, J. Interfacial Solar Vapor Generation: Materials and Structural Design. *Acc. Mater. Res.* **2021**, 2 (4), 198–209.
- (15) Chuang, Y.-H.; Mitch, W. A. Effect of Ozonation and Biological Activated Carbon Treatment of Wastewater Effluents on Formation of N-Nitrosamines and Halogenated Disinfection Byproducts. *Environ. Sci. Technol.* **2017**, *51* (4), 2329–2338.
- (16) Szczuka, A.; Parker, K. M.; Harvey, C.; Hayes, E.; Vengosh, A.; Mitch, W. A. Regulated and Unregulated Halogenated Disinfection Byproduct Formation from Chlorination of Saline Groundwater. *Water Res.* **2017**, *122*, 633–644.
- (17) Sun, M.; Wang, X.; Winter, L. R.; Zhao, Y.; Ma, W.; Hedtke, T.; Kim, J.-H.; Elimelech, M. Electrified Membranes for Water Treatment Applications. *ACS EST Eng.* **2021**, *1* (4), 725–752.
- (18) Guo, L.; Ding, K.; Rockne, K.; Duran, M.; Chaplin, B. P. Bacteria Inactivation at a Sub-Stoichiometric Titanium Dioxide Reactive Electrochemical Membrane. *J. Hazard. Mater.* **2016**, 319, 137–146.
- (19) Kotnik, T.; Frey, W.; Sack, M.; Haberl Meglič, S.; Peterka, M.; Miklavčič, D. Electroporation-Based Applications in Biotechnology. *Trends Biotechnol* **2015**, 33 (8), 480–488.
- (20) Schoenbach, K. H.; Joshi, R. P.; Stark, R. H.; Dobbs, F. C.; Beebe, S. J. Bacterial Decontamination of Liquids with Pulsed Electric Fields. *IEEE Trans. Dielectr. Electr. Insul.* **2000**, *7* (5), 637–645.
- (21) Gehl, J. Electroporation: Theory and Methods, Perspectives for Drug Delivery, Gene Therapy and Research. *Acta Physiol. Scand.* **2003**, *177* (4), 437–447.
- (22) Yang, C.; Wen, L.; Li, Y.; Li, X. Fabrication of SnO2-Sb Reactive Membrane Electrodes for High-Efficiency Electrochemical Inactivation of Bacteria and Viruses in Water. *Chem. Eng. J.* **2022**, 446, 137327.
- (23) Mahmoud, M.; El-Liethy, M. A. Three-Dimensional, Flowthrough Silver-Magnetite Nanocomposite—Modified Reactive Electrochemical System with Slow Silver Ions Release for Efficient Bacterial Disinfection of Sewage. *J. Environ. Chem. Eng.* **2022**, *10* (1), 106985.
- (24) Liang, S.; Lin, H.; Habteselassie, M.; Huang, Q. Electrochemical Inactivation of Bacteria with a Titanium Sub-Oxide Reactive Membrane. *Water Res.* **2018**, *145*, 172–180.
- (25) Wang, C.; Yue, L.; Wang, S.; Pu, Y.; Zhang, X.; Hao, X.; Wang, W.; Chen, S. Role of Electric Field and Reactive Oxygen Species in Enhancing Antibacterial Activity: A Case Study of 3D Cu Foam Electrode with Branched CuO–ZnO NWs. *J. Phys. Chem. C* **2018**, 122 (46), 26454–26463.
- (26) Huo, Z.-Y.; Zhou, J.-F.; Wu, Y.; Wu, Y.-H.; Liu, H.; Liu, N.; Hu, H.-Y.; Xie, X. A Cu3P Nanowire Enabling High-Efficiency, Reliable, and Energy-Efficient Low-Voltage Electroporation-Inactivation of Pathogens in Water. *J. Mater. Chem. A* **2018**, *6* (39), 18813–18820.
- (27) Huo, Z.-Y.; Xie, X.; Yu, T.; Lu, Y.; Feng, C.; Hu, H.-Y. Nanowire-Modified Three-Dimensional Electrode Enabling Low-Voltage Electroporation for Water Disinfection. *Environ. Sci. Technol.* **2016**, *50* (14), 7641–7649.
- (28) Schoen, D. T.; Schoen, A. P.; Hu, L.; Kim, H. S.; Heilshorn, S. C.; Cui, Y. High Speed Water Sterilization Using One-Dimensional Nanostructures. *Nano Lett.* **2010**, *10* (9), 3628–3632.
- (29) Huo, Z.-Y.; Li, G.-Q.; Yu, T.; Lu, Y.; Sun, H.; Wu, Y.-H.; Yu, C.; Xie, X.; Hu, H.-Y. Impact of Water Quality Parameters on Bacteria Inactivation by Low-Voltage Electroporation: Mechanism and Control. *Environ. Sci. Water Res. Technol.* **2018**, 4 (6), 872–881.
- (30) Huo, Z.-Y.; Liu, H.; Wang, W.-L.; Wang, Y.-H.; Wu, Y.-H.; Xie, X.; Hu, H.-Y. Low-Voltage Alternating Current Powered Polydop-

- amine-Protected Copper Phosphide Nanowire for Electroporation-Disinfection in Water. J. Mater. Chem. A 2019, 7 (13), 7347–7354.
- (31) Yue, L.; Chen, S.; Wang, S.; Wang, C.; Hao, X.; Cheng, Y. F. Water Disinfection Using Ag Nanoparticle—CuO Nanowire Co-Modified 3D Copper Foam Nanocomposites in High Flow under Low Voltages. *Environ. Sci. Nano* **2019**, *6* (9), 2801–2809.
- (32) Huang, Y.; Guo, J.; Li, Y.; Li, H.; Fan, D. E. 2D-Material-Integrated Micromachines: Competing Propulsion Strategy and Enhanced Bacterial Disinfection. *Adv. Mater.* **2022**, 34 (30), 2203082.
- (33) Zhang, Z.; Wang, L.; Chan, T. K. F.; Chen, Z.; Ip, M.; Chan, P. K. S.; Sung, J. J. Y.; Zhang, L. Micro-/Nanorobots in Antimicrobial Applications: Recent Progress, Challenges, and Opportunities. *Adv. Healthc. Mater.* **2022**, *11* (6), 2101991.
- (34) Guo, J.; Liang, Z.; Huang, Y.; Kim, K.; Vandeventer, P.; Fan, D. Acceleration of Biomolecule Enrichment and Detection with Rotationally Motorized Opto-Plasmonic Microsensors and the Working Mechanism. ACS Nano 2020, 14 (11), 15204–15215.
- (35) Ratna, R. V. Economic Analysis of Health Impacts in Developing Countries☆. In *Encyclopedia of Environmental Health*, 2nd ed., Nriagu, J., Ed.; Elsevier: Oxford, 2019; pp 221–230. DOI: 10.1016/B978-0-12-409548-9.10939-X.
- (36) Cisneros, B. J. 4.06 Safe Sanitation in Low Economic Development Areas. In *Treatise on Water Science*, Wilderer, P., Ed.; Elsevier: Oxford, 2011; pp 147–200. DOI: 10.1016/B978-0-444-53199-5.00082-8.
- (37) Herman, J. S.; Gellasch, C. A. Geohydrology: Hydrogeochemistry. In *Encyclopedia of Geology*, 2nd ed., Alderton, D.; Elias, S. A., Eds.; Academic Press: Oxford, 2021; pp 416–425. DOI: 10.1016/B978-0-12-409548-9.12504-7.
- (38) Liang, Z.; Teal, D.; Fan, D. Light Programmable Micro/Nanomotors with Optically Tunable in-Phase Electric Polarization. *Nat. Commun.* **2019**, *10* (1), 5275.
- (39) Pohl, H. A. Dielectrophoresis: The Behavior of Neutral Matter in Nonuniform Electric Fields; Cambridge Monographs on Physics; Cambridge University Press: Cambridge, 1978.
- (40) Morgan, H.; Green, N. G. AC Electrokinetics Colloids and Nanoparticles; Microtechnologies and microsystems series; Research Studies Press, 2003.
- (41) Liang, Z.; Fan, D. Versatile Microparticle Propulsion System by Light-Guided Dielectrophoresis: Proposed Method and Theoretical Calculation. *J. Appl. Phys.* **2021**, *130* (5), 054902.
- (42) Fernádez-Morales, F. H.; Duarte, J. E.; Samitier-Martí, J. Bacterial Handling under the Influence of Non-Uniform Electric Fields: Dielectrophoretic and Electrohydrodynamic Effects. *An. Acad. Bras. Ciênc.* **2008**, *80*, 627–638.
- (43) Park, S.; Zhang, Y.; Wang, T.-H.; Yang, S. Continuous Dielectrophoretic Bacterial Separation and Concentration from Physiological Media of High Conductivity. *Lab. Chip* **2011**, *11* (17), 2893–2900.
- (44) Li, W.; Tekell, M. C.; Liu, C.; Hethcock, J. A.; Fan, D. Flexible All-Solid-State Supercapacitors of High Areal Capacitance Enabled by Porous Graphite Foams with Diverging Microtubes. *Adv. Funct. Mater.* **2018**, 28 (29), 1800601.
- (45) Li, W.; Xu, X.; Liu, C.; Tekell, M. C.; Ning, J.; Guo, J.; Zhang, J.; Fan, D. Ultralight and Binder-Free All-Solid-State Flexible Supercapacitors for Powering Wearable Strain Sensors. *Adv. Funct. Mater.* **2017**, 27 (39), 1702738.
- (46) Chen, Z.; Ren, W.; Gao, L.; Liu, B.; Pei, S.; Cheng, H.-M. Three-Dimensional Flexible and Conductive Interconnected Graphene Networks Grown by Chemical Vapour Deposition. *Nat. Mater.* **2011**, *10* (6), 424–428.
- (47) Hu, G.; Xu, C.; Sun, Z.; Wang, S.; Cheng, H.-M.; Li, F.; Ren, W. 3D Graphene-Foam—Reduced-Graphene-Oxide Hybrid Nested Hierarchical Networks for High-Performance Li—S Batteries. *Adv. Mater.* **2016**, 28 (8), 1603–1609.
- (48) Li, X.; Cai, W.; An, J.; Kim, S.; Nah, J.; Yang, D.; Piner, R.; Velamakanni, A.; Jung, I.; Tutuc, E.; Banerjee, S. K.; Colombo, L.; Ruoff, R. S. Large-Area Synthesis of High-Quality and Uniform

- Graphene Films on Copper Foils. Science 2009, 324 (5932), 1312-1314.
- (49) Li, X.; Colombo, L.; Ruoff, R. S. Synthesis of Graphene Films on Copper Foils by Chemical Vapor Deposition. *Adv. Mater.* **2016**, 28 (29), 6247–6252.
- (50) Guo, J.; Chan, A.; Li, W.; Fan, D. L. Kirkendall Effect in Creating Three-Dimensional Metal Catalysts for Hierarchically Porous Ultrathin Graphite with Unique Properties. *Chem. Mater.* **2017**, 29 (11), 4991–4998.
- (51) Shahini, M.; Yeow, J. T. W. Cell Electroporation by CNT-Featured Microfluidic Chip. *Lab. Chip* **2013**, *13* (13), 2585–2590.
- (52) Sanchis, A.; Brown, A. P.; Sancho, M.; Martínez, G.; Sebastián, J. L.; Muñoz, S.; Miranda, J. M. Dielectric Characterization of Bacterial Cells Using Dielectrophoresis. *Bioelectromagnetics* **2007**, 28 (5), 393–401.
- (53) Valero, A.; Braschler, T.; Renaud, P. A Unified Approach to Dielectric Single Cell Analysis: Impedance and Dielectrophoretic Force Spectroscopy. *Lab. Chip* **2010**, *10* (17), 2216–2225.
- (54) Hoettges, K. F. Dielectrophoresis as a Cell Characterisation Tool. *Microengineering in Biotechnology* **2010**, 583, 183–198.
- (55) Afshar, S.; Salimi, E.; Braasch, K.; Butler, M.; Thomson, D. J.; Bridges, G. E. Multi-Frequency DEP Cytometer Employing a Microwave Sensor for Dielectric Analysis of Single Cells. *IEEE Trans. Microw. Theory Technol.* **2016**, *64* (3), 991–998.
- (56) Huang, E.; White, T.; Wang, B.; Shi, H.; Liu, J. Disinfection of Escherichia Coli by a Reactive Electrochemical Membrane System Involving Activated Carbon Fiber Cloth (ACFC). *Water* **2019**, *11* (3), 430.
- (57) Masliyah, J.; Bhattacharjee, S. Fundamental Transport Equations. In *Electrokinetic and Colloid Transport Phenomena*; John Wiley & Sons, Ltd: Hoboken, NJ, 2006; pp 179–220. DOI: 10.1002/0471799742.ch6.
- (58) Pethig, R. R. Dielectrophoresis: Theory, Methodology and Biological Applications; John Wiley & Sons: Hoboken, NJ, 2017.
- (59) Li, J.; Du, M.; Lv, G.; Zhou, L.; Li, X.; Bertoluzzi, L.; Liu, C.; Zhu, S.; Zhu, J. Interfacial Solar Steam Generation Enables Fast-Responsive, Energy-Efficient, and Low-Cost Off-Grid Sterilization. *Adv. Mater.* **2018**, 30 (49), 1805159.
- (60) Peng, B.; Gao, Y.; Lyu, Q.; Xie, Z.; Li, M.; Zhang, L.; Zhu, J. Cationic Photothermal Hydrogels with Bacteria-Inhibiting Capability for Freshwater Production via Solar-Driven Steam Generation. ACS Appl. Mater. Interfaces 2021, 13 (31), 37724–37733.
- (61) Li, H.; Zhu, W.; Li, M.; Li, Y.; Kwok, R. T. K.; Lam, J. W. Y.; Wang, L.; Wang, D.; Tang, B. Z. Side Area-Assisted 3D Evaporator with Antibiofouling Function for Ultra-Efficient Solar Steam Generation. *Adv. Mater.* **2021**, 33 (36), 2102258.
- (62) Hashim, K. S.; Ali, S. S. M.; AlRifaie, J. K.; Kot, P.; Shaw, A.; Al Khaddar, R.; Idowu, I.; Gkantou, M. Escherichia Coli Inactivation Using a Hybrid Ultrasonic—Electrocoagulation Reactor. *Chemosphere* **2020**, 247, 125868.
- (63) Amabilis-Sosa, L. E.; Vázquez-López, M.; Rojas, J. L. G.; Roé-Sosa, A.; Moeller-Chávez, G. E. Efficient Bacteria Inactivation by Ultrasound in Municipal Wastewater. *Environments* **2018**, 5 (4), 47.
- (64) Malvestiti, J. A.; Cruz-Alcalde, A.; López-Vinent, N.; Dantas, R. F.; Sans, C. Catalytic Ozonation by Metal Ions for Municipal Wastewater Disinfection and Simulataneous Micropollutants Removal. *Appl. Catal. B Environ.* **2019**, 259, 118104.
- (65) Gomes, J.; Frasson, D.; Quinta-Ferreira, R. M.; Matos, A.; Martins, R. C. Removal of Enteric Pathogens from Real Wastewater Using Single and Catalytic Ozonation. *Water* **2019**, *11* (1), 127.
- (66) Chen, Y.; Duan, X.; Zhou, X.; Wang, R.; Wang, S.; Ren, N.; Ho, S.-H. Advanced Oxidation Processes for Water Disinfection: Features, Mechanisms and Prospects. *Chem. Eng. J.* **2021**, *409*, 128207.
- (67) Pronk, W.; Ding, A.; Morgenroth, E.; Derlon, N.; Desmond, P.; Burkhardt, M.; Wu, B.; Fane, A. G. Gravity-Driven Membrane Filtration for Water and Wastewater Treatment: A Review. *Water Res.* **2019**, *149*, 553–565.
- (68) Yang, J.; Monnot, M.; Ercolei, L.; Moulin, P. Membrane-Based Processes Used in Municipal Wastewater Treatment for Water Reuse:

- State-Of-The-Art and Performance Analysis. Membranes 2020, 10 (6),
- (69) Joss, A.; Siegrist, H.; Ternes, T. A. Are We about to Upgrade Wastewater Treatment for Removing Organic Micropollutants? Water Sci. Technol. 2008, 57 (2), 251-255.
- (70) Nyangaresi, P. O.; Qin, Y.; Chen, G.; Zhang, B.; Lu, Y.; Shen, L. Comparison of UV-LED Photolytic and UV-LED/TiO2 Photocatalytic Disinfection for Escherichia Coli in Water. Catal. Today 2019, 335, 200-207.
- (71) Wan, Q.; Cao, R.; Wen, G.; Xu, X.; Xia, Y.; Wu, G.; Li, Y.; Wang, J.; Xu, H.; Lin, Y.; Huang, T. Efficacy of UV-LED Based Advanced Disinfection Processes in the Inactivation of Waterborne Fungal Spores: Kinetics, Photoreactivation, Mechanism and Energy Requirements. Sci. Total Environ. 2022, 803, 150107.
- (72) Nyangaresi, P. O.; Qin, Y.; Chen, G.; Zhang, B.; Lu, Y.; Shen, L. Effects of Single and Combined UV-LEDs on Inactivation and Subsequent Reactivation of E. Coli in Water Disinfection. Water Res. 2018, 147, 331-341.
- (73) Li, X.; Cai, M.; Wang, L.; Niu, F.; Yang, D.; Zhang, G. Evaluation Survey of Microbial Disinfection Methods in UV-LED Water Treatment Systems. Sci. Total Environ. 2019, 659, 1415–1427.
- (74) Wang, Y.; Li, A.; Cui, C. Remediation of Heavy Metal-Contaminated Soils by Electrokinetic Technology: Mechanisms and Applicability. Chemosphere 2021, 265, 129071.
- (75) Rajendran, S.; Priya, T. A. K.; Khoo, K. S.; Hoang, T. K. A.; Ng, H.-S.; Munawaroh, H. S. H.; Karaman, C.; Orooji, Y.; Show, P. L. A Critical Review on Various Remediation Approaches for Heavy Metal Contaminants Removal from Contaminated Soils. Chemosphere 2022, 287, 132369.
- (76) Acar, Y. B.; Gale, R. J.; Alshawabkeh, A. N.; Marks, R. E.; Puppala, S.; Bricka, M.; Parker, R. Electrokinetic Remediation: Basics and Technology Status. J. Hazard. Mater. 1995, 40 (2), 117-137.
- (77) Martínez-Huitle, C. A.; Panizza, M. Electrochemical Oxidation of Organic Pollutants for Wastewater Treatment. Curr. Opin. Electrochem. 2018, 11, 62-71.

□ Recommended by ACS

The Role of Inorganic and Carbon Nanomaterials in Surface **Modification to Attain Antibiofouling Polymeric Membranes** for Water Treatment-A Review

Nkosingiphile E. Zikalala, Malik Maaza, et al.

JUNE 06, 2023

INDUSTRIAL & ENGINEERING CHEMISTRY RESFARCH

RFAD 🗹

Electrospun Polyurethane Nanofiber Membranes for Microplastic and Nanoplastic Separation

Kandiyil Juraij, Athiyanathil Sujith, et al.

MARCH 13, 2023

ACS APPLIED NANO MATERIALS

READ 1

Ultrasmall Cu₃(PO₄), Nanoparticles Reinforced Hydrogel Membrane for Super-antifouling Oil/Water Emulsion **Separation**

Yuyue Mo, Jian Jin, et al.

DECEMBER 07, 2022

ACS NANO

READ C

Wetting-Induced Water Promoted Flow on Tunable Liquid-Liquid Interface-Based Nanopore Membrane System

Yadong Wu, Liping Wen, et al.

JUNE 17, 2022

ACS NANO

READ 🗹

Get More Suggestions >